JOURNAL OF COMPUTATIONAL PHYSICS 55, 408–425 (1984)

Mass Diffusion through a Moving Interface Using a Moving Finite Element Mesh

R. W. S. FOULSER

Atomic Energy Authority, AEE Winfrith, Dorchester, Dorset DT2 8DH, England

Received June 8, 1983; revised December 8, 1983

A one-dimensional finite element method is described for computing the mass diffusion of a chemical species through a domain of two fluids in contact with each other. Within each region coupled binary convection-diffusion equations are satisfied. Concentration jump conditions are imposed across the interface. The interface is allowed to move, obeying a differential equation similar to that encountered in the Stefan problem. Two-dimensional finite elements are used in the space-time plane. These are allowed to evolve so as to maintain an element boundary along the moving interface. The discretization is based on bilinear finite elements in a local coordinate system. Example calculations and calculations to study convergence of the algorithm are described.

1. INTRODUCTION

Enhanced oil recovery (EOR) involves injecting fluids into an oil reservoir and, by contacting the oil with the fluid, releasing oil that would not otherwise be recovered from the rock matrix. This contact is brought about on the bulk scale by the convection of the fluids through the reservoir and this is modelled in large multi-dimensional simulators used to study EOR methods. These simulators usually assume thermodynamic equilibrium between the oil and injected fluids. However, on the pore scale such equilibrium may be achieved only slowly as the result of diffusion-controlled processes. The model described in this paper has been developed to study this aspect of EOR.

The oil in the reservoir is assumed to be trapped in a one-dimensional pore and insulated from the injected EOR fluid by a barrier of water through which the EOR fluid must diffuse to interact with the oil. The oil swells as a result of absorption of the EOR fluid causing the water barrier to be displaced and eroded by the EOR fluid flowing outside the oil-containing pore (see Fig. 1).

The problem of calculating the chemical concentrations and interface motion is related to the Stefan problem with chemical concentrations replacing temperature and concentration jump conditions at the oil/water interface replacing a fixed temperature at the melting front. Bird *et al.* describe the convection-diffusion equations satisfied by a chemical species [1]. In the present application the convection results from density and volume changes that arise because of the changing composition of the fluid

0021-9991/84 $3.00

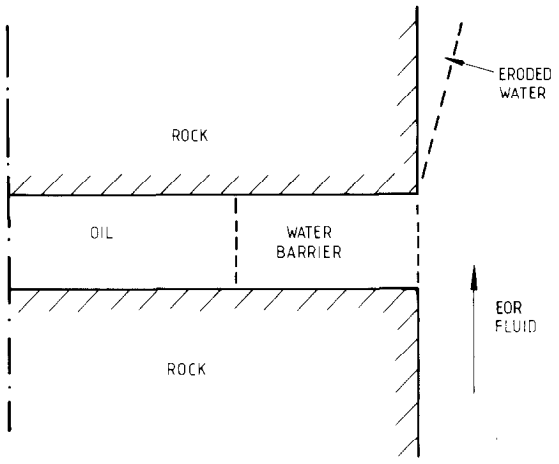

FIG. 1. One-dimensional pore model.

mixtures. This introduces a coupling into the problem not present in the simpler Stefan problem.

Bonnerot and Jamet have reported using finite element calculation models for the solution of the Stefan problem [2–4]. Space-time finite elements were used with a time evolution of the elements chosen so that an element edge was oriented along the melting boundary. The models represented only the region to one side of the melting front.

Varoglu and Finn used the same metod for the solution of the convection-diffusion equation [5]. Characteristics were used to define the evolution of the element boundaries as this largely eliminated oscillations, overshoots and numerical dispersion in the calculation of convection-dominated flows.

The method described in this paper is a development of the work described above. As in the Stefan problem the space-time finite elements are chosen so that an element edge lies along the moving boundary but the regions on both sides of the interface are represented. As will be seen, the boundary moves at a different velocity from the mass average velocity appearing in the convection-diffusion equation so that the characteristic method of Varoglu could only be employed by considering the regions on either side of the interface separately. For the present this has not proved necessary and the element boundaries within the two regions have been moved according to an arbitrary recipe. The conditions at the moving interface are more complicated than those of the Stefan problem and an alternative treatment to that used by Bonnerot and Jamet has been devised.

2. Description of the Problem

We take component 1 to be oil, component 2 to be water and component 3 to be the EOR fluid. Components 1 and 2 are assumed to be mutually insoluble so that only binary mixtures have to be considered. Bird *et al.* [1] derive the convection-diffusion equations used below to describe mass transport in these binary mixtures.

$$\frac{\partial \rho_i}{\partial t} + \frac{\partial n_i}{\partial x} = 0, \qquad \begin{matrix} i = 1, 3, & 0 < x < a(t), & t > 0 \\ i = 2, 3, & a(t) < x < L, & t > 0 \end{matrix} \tag{1}$$

with

$$\begin{aligned} n_i &= \rho_i v - \rho D_1 \frac{\partial(\rho_i/\rho)}{\partial x}, \qquad i = 1, 3, \quad 0 < x < a(t), \quad t > 0 \\ n_i &= \rho_i v - \rho D_2 \frac{\partial(\rho_i/\rho)}{\partial x}, \qquad i = 2, 3, \quad a(t) < x < L, \quad t > 0 \end{aligned} \tag{2}$$

where $\rho_i(x, t)$ is the mass density of component i, $\rho(\rho_1, \rho_2, \rho_3)$ is the total density of the fluid given by an equation of state, $v(x, t)$ is the mass average velocity, $D_j(\rho_1, \rho_2, \rho_3)$ are the binary diffusion coefficients, $a(t)$ is the position of the interface and L is the half-pore length.

There is a compatibility condition

$$\sum_i \rho_i = \rho \tag{3}$$

and the mutual insolubility of components 1 and 2 means that

$$\rho_1(x, t) = 0, \qquad a(t) < x < L \tag{4}$$

$$\rho_2(x, t) = 0, \qquad 0 < x < a(t). \tag{5}$$

An overall balance equation may be obtained by summing Eq. (1) over components and using the compatibility condition to obtain

$$\frac{\partial \rho}{\partial t} + \frac{\partial(\rho v)}{\partial x} = 0. \tag{6}$$

At the interface the component mass densities will not be continuous. For components 1 and 2, Eqs. (4) and (5) impose the interface conditions. For component 3 the size of the discontinuity will be determined by its solubility in components 1 and 2. This may be represented by

$$\rho_3(a(t)^+, t) = \alpha \cdot \rho_3(a(t)^-, t). \tag{7}$$

Equation (7) is the equivalent of assuming the continuity of the mass concentration

of component 3 away from the interface. A mass balance for each component, equivalent to Eq. (1), may be performed around the interface. This results in

$$-\{\rho_i(a(t)^+, t) - \rho_i(a(t)^-, t)\}\frac{da}{dt}$$
$$= n_i(a(t)^+, t) - n_i(a(t)^-, t), \qquad i = 1, 2, 3 \tag{8}$$

which is known as Kotchine's theorem. This, and other interface balance models, is discussed by Slattery [6].

Equation (8) may be summed over components which, after using Eqs. (2) and (3), results in a total density balance, equivalent to Eq. (6), given by

$$-\{\rho(a(t)^+, t) - \rho(a(t)^-, t)\}\frac{da}{dt}$$
$$= \{\rho(a(t)^+, t) \cdot v(a(t)^+, t) - \rho(a(t)^-, t) \cdot v(a(t)^-, t)\}. \tag{9}$$

In general there will be different total densities on both sides of the interface. Hence, from this last equation it may be seen that the mass average velocity will usually undergo a step change at the interface and that the interface velocity, da/dt, will not be the same as the mass average velocity.

The boundary conditions are taken to be

$$\rho_3(L, t) = G(t), \qquad t > 0 \tag{10}$$

$$n_i(0, t) = 0, \qquad i = 1, 2, 3, \quad t > 0 \tag{11}$$

and

$$v(0, t) = 0, \qquad t > 0 \tag{12}$$

and the initial conditions for the model are

$$\rho_3(x, 0) = g(x)$$
$$a(0) = a^0$$

and

$$v(x, 0) = 0.$$

3. Method of Solution

Iteration is necessary to solve the above equation set because of the non-linearities produced by both the product of unknowns ρ_i and v, which occur in Eq. (2), and also because of the moving boundary. Before discussing the finite element formulation we outline below the iteration procedure used to resolve the non-linearities. The procedure is repeated for every timestep.

3.1. *Iterative Solution Method*

(i) Guess average interface velocity da/dt during the timestep (set as the value from previous timestep).

(ii) Guess total density distribution $\{\rho\}$ at the end of the timestep (set as the distribution at the start of the timestep).

(iii) Guess velocity profile $\{v\}$ at the end of the timestep (set as the profile at the start of the timestep).

→ (iv) Find component 3 mass density distribution $\{\rho_3\}$ using Eqs. (1), (2), (7), (8), (10) and (11).

(v) Revise overall density distribution $\{\rho\}$ using $\{\rho_3\}$, Eq. (3) and equation of state for $\rho(\rho_1, \rho_2, \rho_3)$.

(vi) Calculate new velocity profile $\{v\}$ using (6), (9) and (12).

(vii) Calculate new interface velocity da/dt using Eq. (8) for components 1 or 2.

In the calculations performed so far adequate convergence has been achieved using simple iteration in the loop. In the following sections we describe steps in the iteration procedure in more detail.

3.2. *Construction of Q1 Finite Element Basis Functions*

An important feature of the problem posed is the need to represent the interface explicitly in any calculation. Thus, any time-space discretization has to allow the meshes to deform so as to follow the interface. The ability of the finite element method to routinely accommodate irregularly shaped domains may be used to advantage in this type of problem.

In the method the time-space domain is divided into finite elements as shown in Fig. 2. Each quadrangular element can be mapped onto a unit square in the (ξ, η) plane as shown in Fig. 3. Bilinear basis functions are defined in the (ξ, η) space by

$$\begin{aligned}
\phi_1 &= (1-\xi)(1-\eta), && 0 \leqslant \xi \leqslant 1, \quad 0 \leqslant \eta \leqslant 1 \\
\phi_2 &= \xi(1-\eta), && 0 \leqslant \xi < 1, \quad 0 \leqslant \eta \leqslant 1 \\
\phi_3 &= (1-\xi)\eta, && 0 \leqslant \xi \leqslant 1, \quad 0 \leqslant \eta \leqslant 1 \\
\phi_4 &= \xi\eta, && 0 \leqslant \xi < 1, \quad 0 \leqslant \eta \leqslant 1 \\
\phi_j &= 0, && \text{elsewhere} \quad j = 1, 2, 3, 4.
\end{aligned}$$

These are used to define basis functions in the (x, t) plane which are

$$\begin{aligned}
\hat{\phi}^{n-1}_{j+}(x, t) &= \phi_1(\xi, \eta) \\
\hat{\phi}^{n-1}_{(j+1)-}(x, t) &= \phi_2(\xi, \eta) \\
\hat{\phi}^{n}_{j+}(x, t) &= \phi_3(\xi, \eta) \\
\hat{\phi}^{n}_{(j+1)-}(x, t) &= \phi_4(\xi, \eta)
\end{aligned} \qquad \text{where} \qquad (\xi, \eta) = f_j^{-1}(x, t).$$

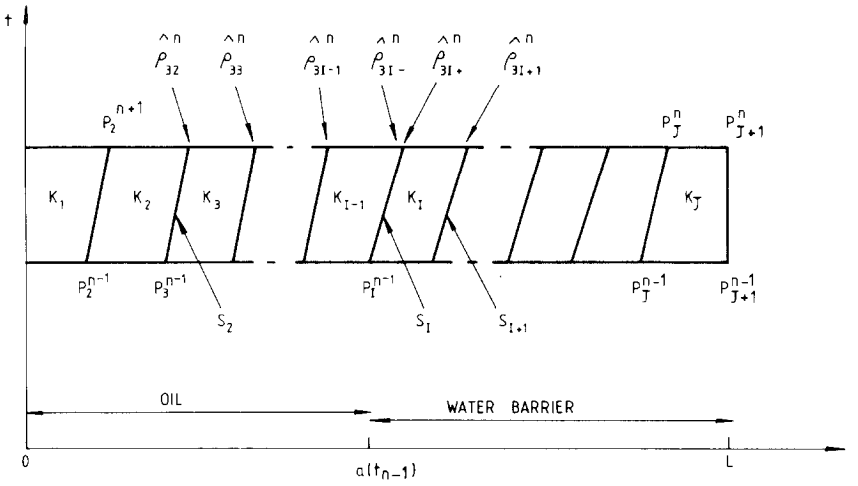

FIG. 2. Finite element set for time interval (t_{n-1}, t_n).

3.3. *Weak Solution for Mass Density of Component* 3

In step (iv) of the algorithm the mass density distribution of component 3 is found. This requires the solution of the convection-diffusion equation represented by Eqs. (1) and (2) subject to the jump conditions in mass density at the interface given by Eq. (7); the balance law around the interface, Eq. (8); and the boundary conditions given by Eqs. (10) and (11).

A weak formulation for solving Eq. (1) for component 3 between two times t^{n-1} and t^n consists of finding $\rho_3 \in H^2[0, L] \times H^1[t^{n-1}, t^n]$ such that

$$\int_{t^{n-1}}^{t_n} \int_0^L \left(\frac{\partial \rho_3}{\partial t} + \frac{\partial n_3}{\partial x} \right) \cdot w \, dx \, dt = 0 \qquad \forall w \in L_2[0, L] \times L_2[t^{n-1}, t^n] \tag{13}$$

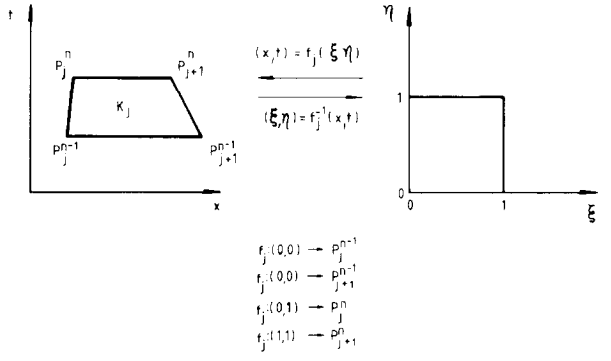

FIG. 3. Mapping of Q_1 elements to unit square in (ξ, η) plane.

where ρ_3 satisfies the boundary conditions at $x=0$ and $x=L$ and the density distribution at the start of the time interval.

The spatial integration domain of Eq. (13) may be split into $(0, a(t))$ and $(a(t), L)$ and an integration by parts performed to obtain

$$\int_{t^{n-1}}^{t^n} \left\{ \int_0^a \frac{\partial \rho_3}{\partial t} w\, dx + [n_3 w]_0^a - \int_0^a n_3 \frac{\partial w}{\partial x}\, dx \right. \\ \left. + \int_a^L \frac{\partial \rho_3}{\partial t} w\, dx + [n_3 w]_a^L - \int_a^L n_3 \frac{\partial w}{\partial x}\, dx \right\} dt = 0. \tag{14}$$

The Neumann boundary condition (11) may be substituted to remove the boundary term at $x=0$. Following normal practice, we also consider only those weighting functions w that vanish at $x=L$ where the Dirichlet boundary condition on ρ_3 is imposed, thus eliminating the boundary term at $x=L$ in Eq. (14). The remaining flux terms at the interface can be eliminated using Eqs. (7) and (8) resulting in a weak formulation in which it is necessary to find $\rho_3 \in H^1 \times H^1$ such that

$$\int_{t^{n-1}}^{t^n} \left\{ \int_0^L \left(\frac{\partial \rho_3}{\partial t} w - n_3 \frac{\partial w}{\partial x} \right) dx + (\alpha - 1)\, \rho_3(a(t)^-, t) \frac{da}{dt} w(a, t) \right\} dt = 0 \\ \forall w \in H_0^1 \times L_2 \tag{15}$$

where the change in function space occurs because of the changed differentiability requirements after integration by parts and the space of weighting functions is limited to those vanishing at $x=L$.

From the above it is clear that we may seek an approximate solution for ρ_3 of the form

$$\hat{\rho}_3 = \sum_{j=1}^{J} (\hat{\rho}_{3_{j+}}^{n-1} \hat{\phi}_{j+}^{n-1} + \hat{\rho}_{3_{(j+1)-}}^{n-1} \hat{\phi}_{(j+1)-}^{n-1} + \hat{\rho}_{3_{j+}}^{n} \hat{\phi}_{j+}^{n} + \hat{\rho}_{3_{(j+1)-}}^{n} \phi_{(j+1)-})$$

with

$$\hat{\rho}_{3_{(j+1)-}}^{k} = G(t^k), \qquad k = n-1, n.$$

The $\hat{\rho}_{3_{j+}}^{k}$ and $\hat{\rho}_{3_{j-}}^{k}$ are values at nodes P_j^k when approached from the right and left, respectively. Where the mass density is continuous these two values are identical; however, at the interface the values may be different.

An obvious choice for a set of weight function $\{w_j\}$ suggested by the Galerkin method is

$$w_j(x, t) = \theta_n(\hat{\phi}_{j+}^{n} + \hat{\phi}_{j-}^{n}) + \theta_{n-1}(\hat{\phi}_{j+}^{n-1} + \hat{\phi}_{j-}^{n-1}), \qquad j = 1, J. \tag{16}$$

For the case where the node positions are constant with time the choice of $\theta_n = -\frac{1}{2}\theta_{n-1}$ would be equivalent to the Faedo–Galerkin formulation with the

resulting set of ordinary differential equations integrated by the normal Euler method. $\theta_{n-1} = -\frac{1}{2}\theta_n$ would correspond to integration using the backward Euler method. $\theta_n = \theta_{n-1} = 1$ time centres the weighting, corresponding to the use of the trapezoidal method, and this has been used in the present model.

Table I summarises the equations generated by the weak formulation of Eq. (15) when the weighting functions (16) are substituted. The integrals have been evaluated by Gauss–Legendre quadrature, to permit high-precision results when variable diffusivities and densities are used. A tridiagonal system of equations results for finding the nodal values $\{\hat{\rho}_{3_j}^n\}$.

3.4. *Weak Solution for Velocity Field*

Step (vi) involves the determination of the velocity field v. This requires the solution of Eq. (6), together with the velocity boundary condition, Eq. (12), and the jump condition, Eq. (9).

TABLE I

$j = 1$	$\int_{K_1}\int \frac{\partial \hat{\rho}_3}{\partial t}(\hat{\phi}_{1+}^{n-1} + \hat{\phi}_{1+}^{n})\,dx\,dt$	
	$+ 0$	$= 0$
	$-\int_{K_1}\int \frac{\partial}{\partial x}(\hat{\phi}_{1+}^{n-1} + \hat{\phi}_{1+}^{n}) \cdot \left(\hat{\rho}_3 \hat{v} - \hat{\rho} D \frac{\partial\left(\frac{\hat{\rho}_3}{\hat{\rho}}\right)}{\partial x}\right) dx\,dt$	
$2 \leqslant j \leqslant I-1$	$\int_{K_{j+1}\cup K_j}\int \frac{\partial \hat{\rho}_3}{\partial t}(\hat{\phi}_{j+}^{n-1} + \hat{\phi}_{j-}^{n-1} + \hat{\phi}_{j+}^{n} + \hat{\phi}_{j-}^{n})\,dx\,dt$	
	$+ 0$	$= 0$
$I+1 \leqslant j \leqslant J$	$-\int_{K_{I-1}\cup K_J}\int \frac{\partial}{\partial x}(\hat{\phi}_{j+}^{n-1} + \hat{\phi}_{j-}^{n-1} + \hat{\phi}_{j+}^{n} + \hat{\phi}_{j-}^{n}) \cdot \left(\hat{\rho}_3 \hat{v} - \hat{\rho} D \frac{\partial\left(\frac{\hat{\rho}_3}{\hat{\rho}}\right)}{\partial x}\right) dx\,dt$	
	$\int_{K_{I-1}\cup K_I}\int \frac{\partial \hat{\rho}_3}{\partial t}(\hat{\phi}_{I+}^{n-1} + \hat{\phi}_{I-}^{n-1} + \hat{\phi}_{I+}^{n} + \hat{\phi}_{I-}^{n})\,dx\,dt$	
$j = I$	$+\int_{t_n}^{t_{n+1}} \hat{\rho}_{3I-}(\alpha - 1)\left(\frac{da}{dt}\right) dt$	$= 0$
	$-\int_{K_{I-1}\cup K_I}\int \frac{\partial}{\partial x}(\hat{\phi}_{I+}^{n-1} + \hat{\phi}_{I-}^{n-1} + \hat{\phi}_{I+}^{n} + \hat{\phi}_{I-}^{n}) \cdot \left(\hat{\rho}_3 \hat{v} - \hat{\rho} D \frac{\partial\left(\frac{\hat{\rho}_3}{\hat{\rho}}\right)}{\partial x}\right) dx\,dt$	

A weak formulation for solving Eq. (6) may be written:
Find $v \in H^1 \times L_2$ such that

$$\int_{t^{n-1}}^{t_n} \int_0^L \left(\frac{\partial \rho}{\partial t} + \frac{\partial(\rho v)}{\partial x} \right) w' \, dx \, dt = 0, \qquad \forall w' \in L_2 \times L_2 \tag{17}$$

where v satisfies the boundary condition $v(0, t) = 0$ and the known velocity field at time t^n.

An approximate solution for v may be sought in the sub-space of $H^1 \times L_2$ where $\hat{v}$ has the form

$$\hat{v} = \sum_{j=1}^{J} \hat{v}^n_{j+} \hat{\phi}^n_{j+} + \hat{v}^n_{(j+1)-} \hat{\phi}^n_{(j+1)-} + \hat{v}^{n-1}_{j+} \hat{\phi}^{n-1}_{j+} + \hat{v}^{n-1}_{(j+1)-} \hat{\phi}^{n-1}_{(j+1)-} \tag{18}$$

with

$$\hat{v}^k_{1+} = v(0, t^k), \qquad k = n-1, n.$$

At most internal nodes the velocity is continuous so that

$$v^k_{j+} = v^k_{j-}, \qquad j \neq 1, I, J+1, k = n-1, n.$$

However, at the interface, $j = I$, the velocity jump condition, Eq. (9) may be used to eliminate one of the two velocities on either side of the discontinuity.

When approximation (17) is substituted into Eq. (18) with J independent weighting functions then a set of equations results for the nodal velocities $\{\hat{v}^n_{j\perp}\}$. If the weighting functions $\{w'_j\}$ are chosen to be those previously used, $\{w_j\}$, then alternate nodal velocities are uncoupled in the resulting equations so that the scheme is unstable. Consequently, an alternative weighting scheme has been used which takes advantage of the larger function space appropriate to this phase of the problem being solved, $L_2 \times L_2$. The assumed weighting functions are

$$w'_j(x, t) = \delta^i_j(\theta_{n-1}(1-\eta) + \theta_n \eta), \qquad j = 1, J$$

where

$$\begin{aligned} \delta^i_j &= 1 \qquad \text{if} \quad i = j \\ &= 0 \qquad \text{if} \quad i \neq j \end{aligned}$$

and

$$(\xi, \eta) = f_j^{-1}(x, t).$$

To obtain a stable scheme for calculations with variable overall density, ρ, we have taken $\theta_{n-1} = \frac{1}{2}\theta n$. This corresponds to using a backward Euler time discretization in a Faedo–Galerkin formulation.

Again the integrals represented by Eq. (17), for each w'_j have been evaluated by Gauss–Legendre quadrature.

3.5. *Finite Element Determination of Interfacial Velocity*

The overall solution algorithm described in Section 3.1 ensures that the mass density distribution of component 3 and the overall velocity/density distributions satisfy the weak forms of their governing equations and interface jump conditions. The mass density distributions of components 1 and 2 can be deduced at step (v) using the compatibility condition given by Eq. (3). However, the corresponding interface jump conditions (8) relating fluxes to interface mass density values for these components will not be satisfied except when the interface motion is correctly predicted. Thus (8) can be used together with the approximate distributions $\hat{\rho}_1$ or $\hat{\rho}_2$ to provide an independent estimate of the interface velocity.

In the application of the model described in this note the position of the interface could have been determined by conservation of the mass of component 1. However, a more general treatment has been sought and the mass conservation used to assess the convergence properties of the algorithm is described in Section 4.2.

Bonnerot and Jamet [2, 4] used a one-sided finite difference approximation to determine the energy flux at the interface in their Stefan problem analysis. This would be equivalent to using one-sided approximations to the two flux terms given by (2) applicable to either side of the moving interface and substituting these into (8). This method has not been adopted in this analysis partly because the use of finite differences in a solution method entirely formulated in terms of a weak formulation was unattractive. Also, to obtain sufficient precision Bonnerot and Jamet incorporated into their finite difference expressions nodal values outside the elements adjacent to the interface, and this is undesirable in the present application where the barrier region may be reduced to a single element in thickness.

For convenience we consider component 1 to derive the interface velocity based on a weak statement. The approximate mass density distribution for component 1 satisfies a set of equations similar to those satisfied by component 3 (see Table I). In particular the equation for the region around the interface, $j = I$, must be satisfied. That is,

$$\int_{K_{I-1}} \frac{\partial \hat{\rho}_1}{\partial t} w_I \, dx \, dt - \int_{t^n}^{t^{n+1}} \hat{\rho}_{1I} - \left(\frac{da}{dt}\right) dt - \int_{K_{I-1}} \frac{\partial w_I}{\partial x} \hat{n}_1 \, dx \, dt = 0.$$

Since $\hat{\rho}_1(x, t)$ is available from step (v) this equation can be used to provide an estimate of da/dt which has been assumed to be constant over the time interval.

3.6. *Element Evolution*

The initial element structure to cover the regions $0 \leqslant x \leqslant a^0$ and $a^0 \leqslant x \leqslant L$ has been chosen in a number of ways, as described in Section 4.2. During the transient the element geometry is modified so that an element boundary lies along the moving interface. Thus, the position of one set of nodes $\{P_I^k\}$ is determined by the initial position of the interface, a^0, and by integration of the interface velocity, da/dt:

$$P_I^k = a(t^k) = a^0 + \int_0^{t^k} \left(\frac{da}{dt}\right) dt = a^0 + \sum_{j=1}^{k-1} \left(\frac{da}{dt}\right)_j (t^{j+1} - t^j).$$

In normal applications of the model the nodes in the oil region $\{P_j^k: 1 < j < I\}$ are chosen so that the intervals (x_j^k, x_{j+1}^k) grow in proportion to the overall length $(0, x_I^k)$ and nodes in the barrier region are moved so that the lengths (x_j^k, x_{j+1}^k) remain constant except for the edge element K_J whose length is reduced. This last element is eliminated and the element K_{J-1} is extended before the element K_J degenerates into a triangular region.

An alternative node-moving strategy is briefly described in Section 4.2 when it is used, in addition to the above, to investigate the convergence of the algorithm.

4. Numerical Calculations

First in this section we describe five calculations which show the behaviour of the model. For one of these examples an approximate analytic solution can be obtained and the agreement between this solution and the numerical solution indicates that the weak formulation of the problem is consistent with the original differential statement. In the second sub-section the convergence and stability of the numerical method is discussed.

4.1. *Example Calculations*

First we consider the effects of changing only the jump condition parameter α. The data for these calculations are:

$$
\begin{aligned}
a^0 &= 1, & I(t=0) &= 8 \\
L &= 2, & J(t=0) &= 16 \\
D_1 &= D_2 = 1, & & \\
\rho(x) &= 700, & 0 &\leqslant x < a(t) \\
&= 1000, & a(t) &< x \leqslant L \\
g(x) &= 0, & & \\
G(t) &= 175, & t &> 0 \\
\alpha &= 0.5;\ 1.0;\ 2.0. &&
\end{aligned}
$$

Figure 4 shows the mass density distribution for component 3 at time = 2. Note the jump in mass density at the interface which is moving from left to right. The interface moves despite the assumption of constant overall density in the two regions because of the addition of mass to the oil region. The time variation of the interface position is shown in Fig. 5. It asymptotes to a position that can be calculated by considering the conservation of mass of component 1. This states that

$$a^0\rho_1^0 = a(\infty)(\rho_1^0 - \alpha G(\infty)) \tag{19}$$

where ρ_1^0 is the density of the oil (700).

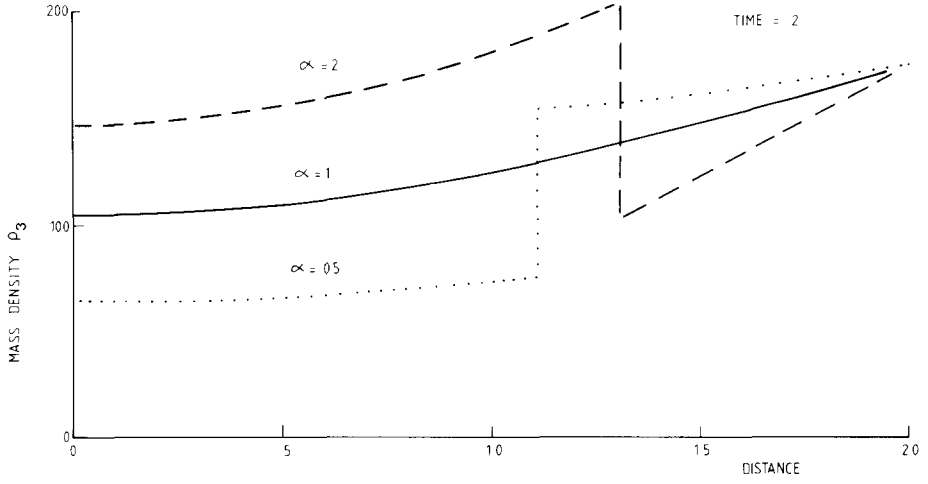

FIG. 4. Example of mass density distributions of component 3. Effect of changing discontinuity jump condition.

It is interesting that the asymptotic position is approached earlier with the smaller α despite the lower mass density gradients which are generated in both regions.

Because in these sample calculations the total fluid densities within each region have been assumed constant, Eq. (6) shows that the mass average velocities in each region are constant. The velocity in the oil region is zero because of the boundary condition represented by Eq. (12). The mass average velocity in the water region is non-zero being related to the interface velocity by Eq. (9). Figure 6 shows the computed velocities for the sample case with $\alpha = 2$, which has the highest velocities.

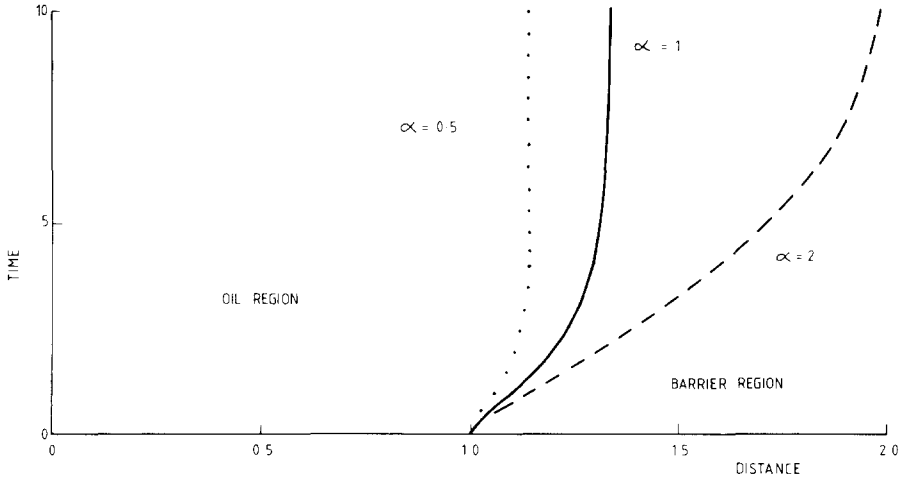

FIG. 5. Example of movement of interface. Effect of changing discontinuity jump condition.

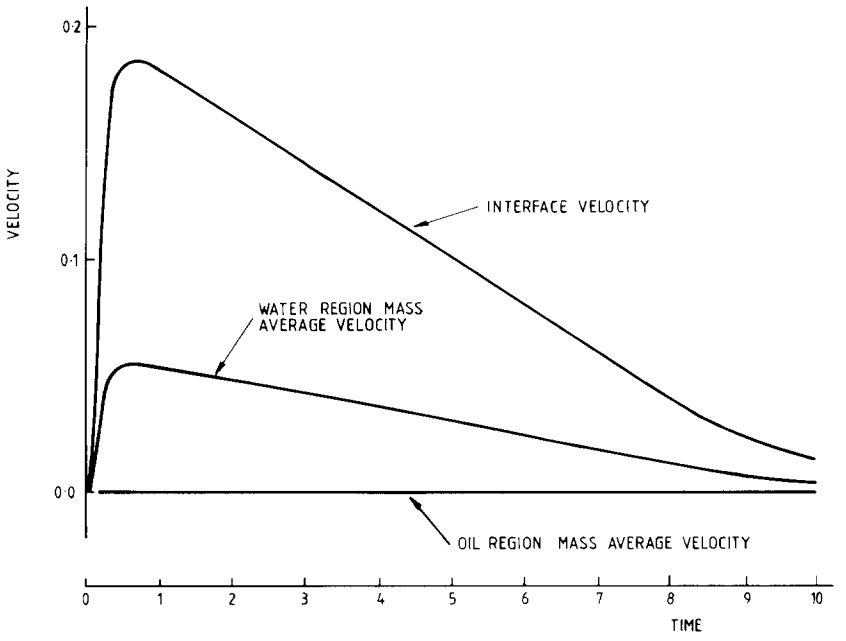

FIG. 6. Interface and mass average velocities for case $\alpha = 2.0$.

As may be seen, the maximum interfacial velocity is 0.185 and the maximum mass average velocity is 0.055. "Wiggles" in the solution would be expected to occur when the fluid moves relative to the mesh to give a cell Reynolds number greater than two. The method of Varoghn and Finn avoided this in convection-dominated flows by moving the mesh at the speed of the fluid. In the present case the meshes were moved at speeds similar to the interface velocity, however, the relative mass average velocities are small enough that the cell Reynolds numbers are well below the stability threshold.

In a second group of example calculations we consider the effect of changing the relative diffusivities in the two regions. The data for these calculations are:

$$
\begin{aligned}
a^0 &= 1, & I(t=0) &= 8 \\
L &= 2, & J(t=0) &= 16 \\
D_1 &= 0.55, \quad D_2 = 5.5; & D_1 &= 5.5, \quad D_2 = 0.55 \\
\rho(x) &= 700, & 0 &\leqslant x < a(t) \\
&= 1000, & a(t) &< x \leqslant L \\
g(x) &= 0, & & \\
G(t) &= 175, & 0 &< t \\
\alpha &= 1.0. &&
\end{aligned}
$$

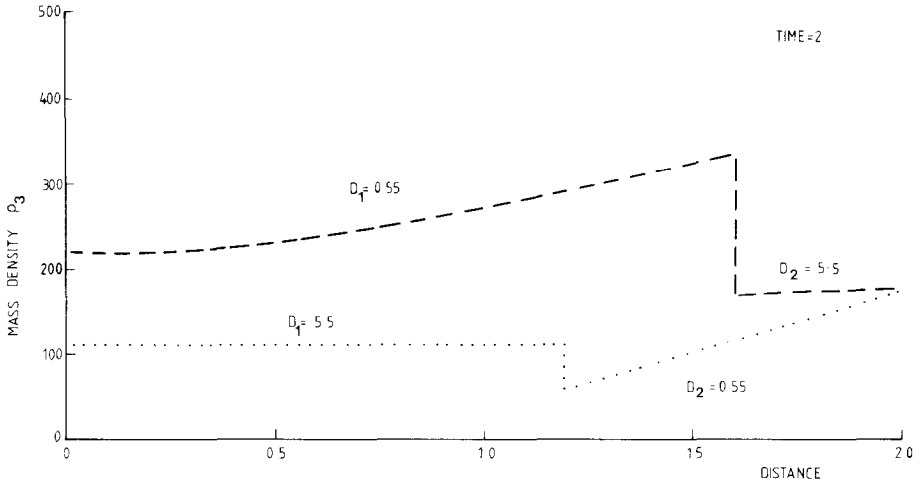

FIG. 7. Example of mass density distribution of component 3. Effect of diffusivity contrasts.

The results of these calculations using these data are shown in Figs. 7 and 8.

With the higher diffusivity in the barrier region the interface rapidly moves towards $L = 2$. The mass density distribution shows that the timescale is being determined by the low rate of mass transfer in the oil region.

With the lower diffusivity in the barrier region the timescale for the interface displacement is extended. The mass of component 3 in the oil is almost constant and the distribution in the barrier region is almost linear. Assuming that these obser-

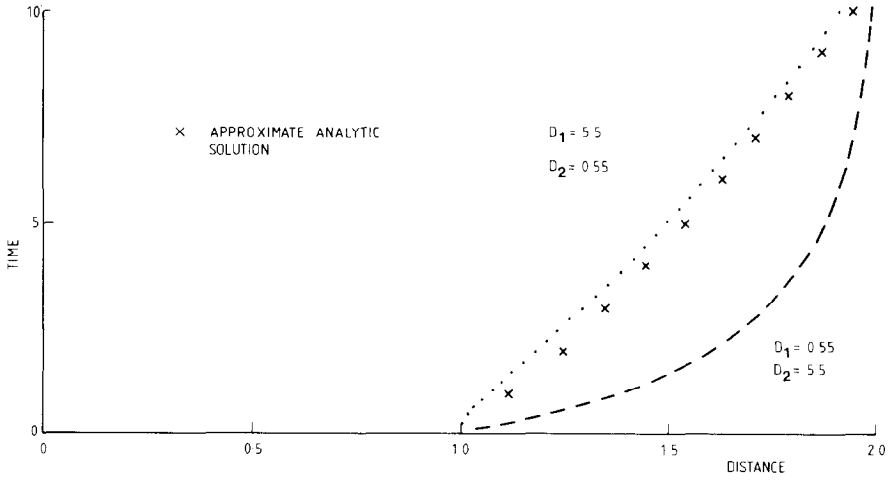

FIG. 8. Example of movement of interface. Effect of diffusivity contrasts.

vations apply exactly from the start of the calculation, the following ordinary differential equation can be derived to describe the motion of the interface:

$$\frac{da}{dt} = \frac{a(\alpha G^0 - \rho_1^0) + a^0 \rho_1^0}{a(L-a)} \cdot \frac{D_1}{\alpha \rho_1^0} \tag{20}$$

where G^0 is the constant boundary value for component 3 and ρ_1^0 is the initial mass density of component 1 in the region $0 \leqslant x < a(t)$; this is assumed to be the same as the overall density in this region at all times. With the example data this equation has the solution

$$a(t) = a^0 + (1 + 0.275 \cdot t)^{1/2}. \tag{21}$$

The position of the interface predicted using this expression has been added to the numerical results shown on Fig. 7. The slight time advance of the analytic expression is mainly due to the time required to establish the linear distribution of components in the barrier region.

4.2. *Convergence and Stability of the Algorithm*

To examine convergence in the Stefan problem Bonnerot and Jamet [2, 4] examined the position of the interface at a fixed time. An analytic result was not available with which to compare the calculated results and so the changes in position of the interface that occurred when three different numbers of elements were used were compared to give an estimate of the order of convergence. This analysis showed that second-order convergence was achieved with Q_1 elements of regular length and third order with Q_2 elements (quadrilateral elements with biquadratic basis functions). A similar analysis applied to temperatures showed the same order of convergence if improved temperatures were obtained by interpolation using a polynomial of one degree higher order than that of the basis functions.

As noted in Section 3.5, the problem tackled in this paper should conserve the overall mass of component 1 though no use is made of this in the solution algorithm. Consequently, the error in the numerical estimation of the mass of this component may be used to study convergence. The integration of the linear piecewise approximation to ρ_3 may be integrated exactly so that the rate of convergence obtained from this method is the same as the rate of pointwise convergence.

The following data, suggested by the Bonnerot–James analysis of the Stefan problem, has been used:

$$\begin{aligned} a^0 &= 1, & I(t=0) &\text{ varied} \\ L &= 2, & J(t=0) &= 2 \times I(t=0) \\ D_1 &= D_2 = 1, & & \\ \rho(x) &= 700, & 0 &\leqslant x < a(t) \\ \rho(x) &= 1000, & a(t) &< x \leqslant L \end{aligned}$$

$$g(x) = 0, \qquad 0 \leqslant x \leqslant a^0$$
$$= 200\left(\frac{x - a^0}{L - a^0}\right)^2, \qquad a^0 < x < L$$
$$G(t) = 200,$$
$$\Delta t = a^0/I(t = 0).$$

First, calculations were done using an element structure which had equally spaced nodes in the regions. These were allowed to evolve in the way described in Section 3.6. Figure 6 shows the variation of the error as a function of the number of elements used in the calculation. The slope of the curve, 2, indicates that the calculation has second-order convergence.

Almost identical results were obtained using elements whose length initially increased arithmetically away from the interface.

Bonnerot and Jamet found that if the nodes in their Q_1 calculations were chosen so that the relative length of the elements was not constant, then the convergence deteriorated from second to first order [2]. To investigate this in the present problem the elements were varied as shown in Fig. 10. The behaviour of the error was plotted in Fig. 9 and this shows that the convergence is unaffected by the irregular spacing. This improvement in behaviour is attributed to the alternative method used to evaluate the interfacial velocity.

The stability of the approximations is indicated by the fact that simple iteration has proved adequate in the outer loops of the solution algorithm described in Section 3.1 (initial errors in a guessed solution are damped out). This has remained true when non-constant overall densities and interfacial density jumps of real systems have been incorporated into calculations of the type described above.

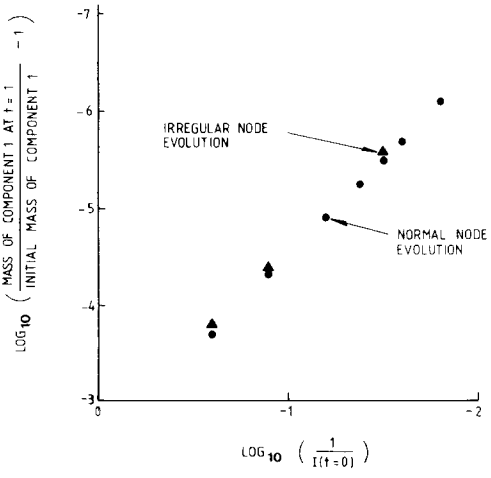

FIG. 9. Evaluation of order of convergence of method.

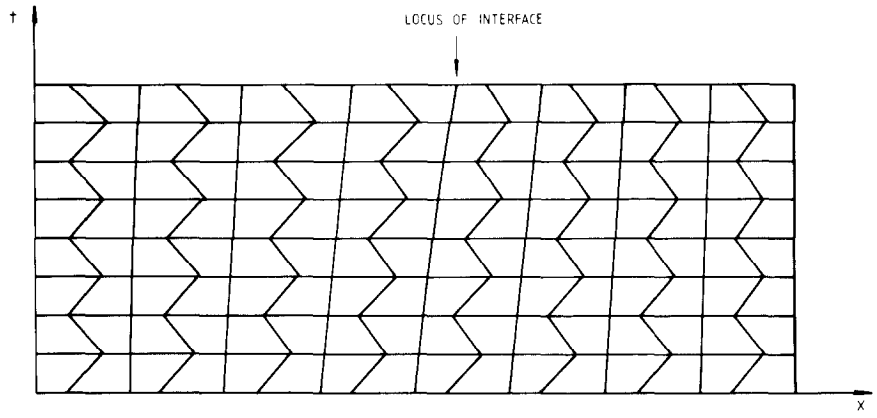

FIG. 10. Irregular node evaluation.

5. CONCLUSIONS

A finite element method was used to calculate mass diffusion in a composite region. Within each of the two regions coupled binary convection-diffusion equations must be solved and the interface between the regions may move. The solution algorithm is iterative, based on solving the convection diffusion equation for one component, an overall continuity equation and calculating the interface movement from a weak statement of the equations satisfied by the diffusing components at the interface. The iterative scheme has proved stable in all the computations performed to date using both simplified and more physically realistic data. The convergence of the method is second order, corresponding to the second-order convergence obtained by Bonnerot and Jamet for the one-dimensional Stefan problem using Q_1 elements, and this second-order convergence is maintained when a non-uniform element evolution is considered. The improved behaviour of the method for irregular elements is attributed to the alternative treatment of the interface considered in this paper. This treatment has the added advantage of involving only those elements immediately adjacent to the interface. The model is currently being further developed to enable the mechanisms of EOR to be investigated on a pore scale.

ACKNOWLEDGMENTS

The author would like to thank those colleagues at AEE Winfrith, particularly Dr. C. L. Farmer, with whom various aspects of this model were discussed. The work reported in this paper has been funded by the UK Department of Energy.

REFERENCES

1. R. B. BIRD, W. E. STEWART, AND E. N. LIGHTFOOT, "Transport Phenomena," Wiley, New York/London, 1960.
2. R. BONNEROT AND P. JAMET, *Internat. J. Numer. Methods Engrg.* **8** (1974), 811–820.
3. R. BONNEROT AND P. JAMET, *J. Comput. Phys.* **25** (1977), 163–181.
4. R. BONNEROT AND P. JAMET, *J. Comput. Phys.* **32** (1979), 145–167.
5. E. VAROGLU AND W. D. FINN, *J. Comput. Phys.* **34** (1980), 371–389.
6. J. SLATTERY, *I & EC Fundamentals* **6** (1967), 108–115.